Simulating Chiral Induced Spin Selectivity using Non-Equilibrium Green's Functions

Tim H.F. Vroomans

October 22, 2019
revised: January 30, 2020

Abstract

In this thesis a method is proposed to improve upon the Non-Self-Consistent Green's function transport calculation used by the Amsterdam Density Functional package (ADF) made by Software for Chemistry and Materials (SCM) [1] [2] [14] so ADF is able to simulate Chiral Induced Spin Selectivity (CISS). CISS is an effect that causes spin polarisation to occur in currents that flow through chiral molecules, such as DNA [7] [19]. In this thesis, Helicene is chosen since it has a helical structure but it is also a relatively simple molecule to simulate. In the calculations the helicene is attached to two gold contacts via a sulfur atom on each side. Gold is chosen for its strong spin-orbit coupling, which is thought to cause the effect.

The native Green's function transport calculation uncouples the spin-orbitals into their two spin directions, it essentially preforms the same calculation twice for both spin direction [13]. Because the spin directions are treated separately this method neglects any interactions between electrons of different spin. Therefore no spin polarisation will arise in the absence of a magnetic field.

The proposed method improves on this by accounting for the full spin-orbitals, and therefore their potential overlap with each other [11]. Because the potential interactions between orbitals occupied by electrons of different spin, spin-flip interactions are taken into account in the Green's function when calculating the transmission of the Helicene. This then gives rise to potential spin polarisation in the current.

Due to a lack of time and an overabundance of run-time errors in the FORTRAN code used to implement the proposed method in ADF 2019, no results could be obtained to confirm or deny this.

Contents

Chapter 1

Introduction

1.1 The discovery of electron spin

In the nineteenth century, physicists were trying to uncover relations between the different forces of nature, and therefore many experiments were aimed at measuring the effects of electromagnetic fields on light. In this fashion it was found that candle light would become polarised if it was affected by magnetic fields [8] and the spectral lines of glowing substances would split if the substance was subjected to an electric field [6], which is called the Kerr effect. In 1896, as a follow-up on his doctoral research on the Kerr effect, Pieter Zeeman was interested in the effect of a magnetic field on the spectral lines of matter [20]. To this end Zeeman heated up some kitchen salt which started to glow with the well known yellow glow of Sodium, made famous by street lights. He then passed the light emitted by the salt through an optical grating to obtain the unique spectral lines of Sodium. When Zeeman placed the salt in the magnetic field of an electromagnet, he would observe that the spectral lines would thicken.

Hendrik Lorentz caught wind of these observations and went on to try and explain these observations using electromagnetic theory. He implied that the spectral lines did not thicken, but split into two or three different spectral lines. These spectral lines were caused by particles which Lorentz called 'Ions of light' which circled around in atoms [17]. Using the Maxwell Equations, Lorentz was not only able to predict the effect Zeeman observed, but he was also able to predict the charge to mass ratio of his 'Ions of light'. Lorentz explained that Zeeman did not observe a split in spectral lines because the resolution of his optical grating was too low. This was confirmed later when Zeeman used Cadmium and he observed the splitting of its spectral lines. In 1897 Joseph John Thomson discovered the electron, which had the charge to mass ratio which Lorentz predicted [3]. And thus it was discovered that Lorentz' 'Ions of light' were actually Thomson's electrons. Using the Zeeman effect the structure of atoms could now be studied.

There was a catch though. When more experiments of the same kind were executed they showed splitting of the spectral lines into more than three new spectral lines. Physicists attributed these extra splittings to the angular momentum of the spinning core of the atom. However, not long after that, Wolfgang Pauli respectfully obliterated this notion in a landslide article [9]. In this article Pauli introduced a fourth quantum number and the theorem that no two electrons could exist in the same quantum state. This is now known as the famous Pauli Exclusion Principle. In 1924 Samuel Goudsmit and George Uhlenbeck introduced the concept of electron spin and showed that this spin was Pauli's fourth quantum number [18]. Because of its spin an electron is not only a tiny electric charge but also a tiny magnetic dipole, causing the electron to behave like a minuscule bar magnet. Adapting the Bohr model for the atom with the electron's spin the Zeeman effect could be explained.

1.2 The applications of electron spin

Electron spin could now describe and explain a whole plethora of phenomena such as atoms with unpaired electrons and spin-orbit coupling, an expression of the Zeeman effect due to the fact that the electrons on the inner orbitals of heavy atoms move so fast that relativistic effects start to become very relevant. One of these effects is that the electric field caused by the nucleus of a heavy atom starts to look like a magnetic field in the reference frame of an electron moving at relativistic speeds. This magnetic field then causes a perturbation on the energy of the electron due to the magnetic dipole produced by its spin. But other than some symmetry constraints it was not important for closed-shell systems such as hydrocarbons which have a very small Spin-Orbit coupling.

In the 1980's the notion of "spintronics" was conceived of. In spintronics spins are used as quantum bits to transfer information and preform calculations. Generally this is associated with inorganic matter, such as metals, semiconductors and oxides. But if organic molecules could be used it would have several advantages because of their, ease of production, flexibility, compatibility with biologic systems and, not entirely unimportant, low cost. Some headway has been made in incorporating organic molecules in spintronics, but only when adsorbed to a (ferro)magnetic substrate [7].

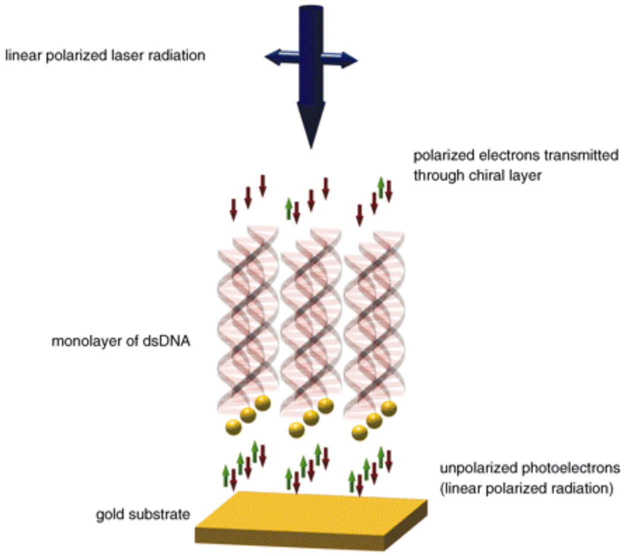

Figure 1.1: The experimental set-up used in [4]

.

1.2.1 Chiral Induced Spin Selectivity

It was quite the surprise that in relatively recent research by Goheler et al. [4] and Xie et al. [19] unusually high spin polarisation was measured of photoelectrons and tunneling currents through chiral organic molecules. This effect is now called Chiral Induced Spin Selectivity (CISS). The spin polarisation was calculated as:

$$P = \frac{j_\uparrow - j_\downarrow}{j_\uparrow + j_\downarrow}, \tag{1.1}$$

where $j_\uparrow$ is the current associated with spin-up electrons and $j_\downarrow$ is the current associated with spin-down electrons. Chiral molecules are molecules which cannot be superimposed on their mirror image, and thus do not posses parity symmetry. Similarly as to how our hands cannot be superimposed onto each-other. Which is where chirality (derived from the Greek word for hand) gets its name.

An example of this is DNA with its famous double-helix structure. If one would take two DNA strands with identical base-structure, but one strand would turn clockwise and the other strand would turn counter-clockwise, taking the mirror image of one would not make the strand identical to the other strand. Convincing observation of CISS were done by Xie et al and Gohler et al by transmitting photo-electrons through self-assembled monolayers of DNA. The latter experiment gives a very convincing result of CISS. The experimental set-up of Gohler et al can be seen in Figure 1.1. First

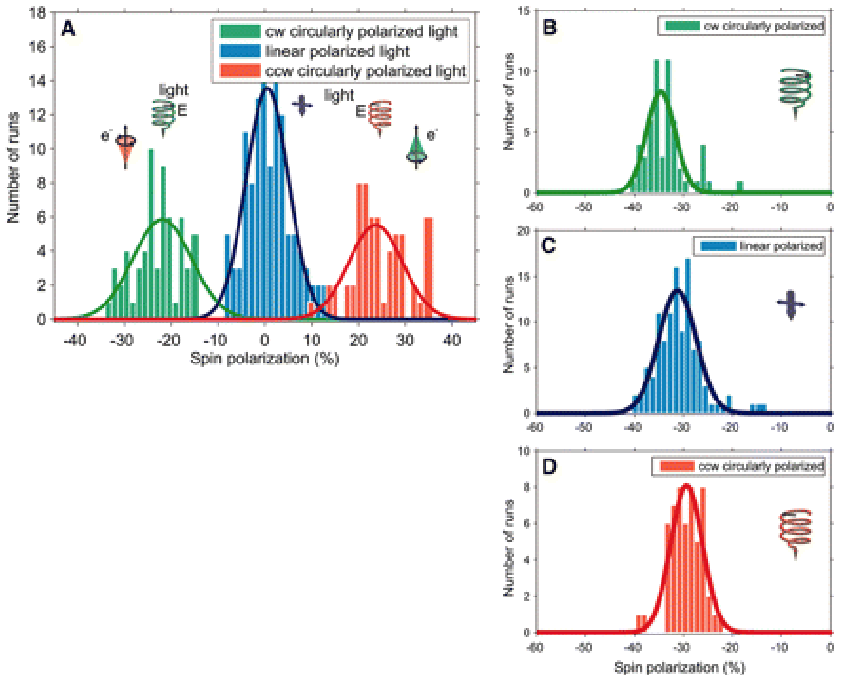

Figure 1.2: The results obtained from the experiments performed in [4] on a single-crystal Au(111) substrate. Figure A shows the results from the control experiment. Figures B through D show the experiments performed with the dsDNA attached to the substrate. The former figures show the results for cw circularly polarised light (B), linearly polarised light (C) and ccw circularly polarised light (D). The x-axes are in terms of the spin polarisation in percentages, the y-axes are in terms of the amount of runs a specific P was obtained.

a control experiment was performed on a bare single-crystal Au(111) or poly-crystalline Au substrate in which, under high vacuum conditions, linearly polarised light, clockwise circularly polarised light or counterclockwise circularly polarised light from a laser is shone onto the gold substrate to knock loose photo-electrons from the substrate. Their polarisation is measured using either a Mott polarimeter or a time-of-flight instrument which records the kinetic-energy distribution of the photo-electrons. Then, strands of double-stranded DNA (dsDNA) are thiol bonded to the substrate of either single-crystal Au(111) or poly-crystalline Au to create a self-assembled mono-layer of dsDNA. The laser is again shone on the substrate and now the photo-electrons have to travel through the self-assembled mono-layer of dsDNA and their polarisation is again measured. The results performed with the single-crystal Au(111) substrate can be seen in Figure 1.2. During

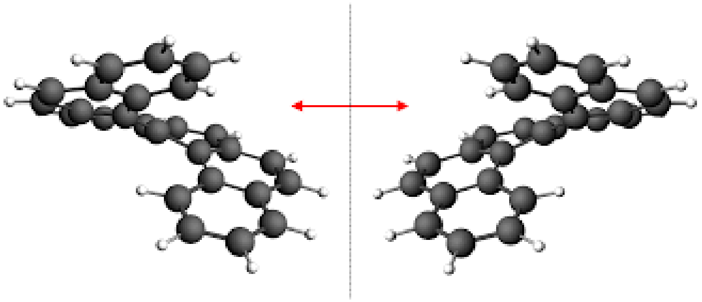

Figure 1.3: A counterclockwise and a clockwise Helicene molecule. As can be seen from the Figure, the two mirror images cannot be superimposed onto one-another. [11]

the control experiment (Figure 1.2.A) the results are as expected: no spin polarisation is measured when using linearly polarised light and spin polarisation is measured when circularly polarised light is used. But when the self-assembled mono-layer of dsDNA is attached to the substrate a mean polarisation of $\langle P \rangle = -31\%$ was measured for linearly polarised light (Figure 1.2.C), $\langle P \rangle = -35\%$ for clockwise circularly polarised light (Figure 1.2.B) and $\langle P \rangle = -29\%$ for counterclockwise circularly polarised light (Figure 1.2.D). When the dsDNA is attached to poly-crystalline Au the effect is stronger and the mean polarisation takes the approximate value $\langle P \rangle = -60\%$. This is a clear indication that the chiral dsDNA molecules induce spin polarisation.

A simpler molecule with a helical structure is Helicene. In Figure 1.3 its chiral nature can be seen. 4-Helicene, a Helicene strand consisting of four benzene rings ”knitted” together, is used in the calculations in this thesis. It is the goal of the research that leads to this thesis to be able to simulate the Chiral Induced Spin Selectivity effect using the ADF software developed by SCM [1].

1.3 Structure of this thesis

In the next chapter of this thesis the relevant theory to this research will be introduced. In the third chapter the methods used will be explained and in the fourth chapter the results obtained will be presented, and in the last chapter a brief discussion of the results will be followed-up by a conclusion.

This research was executed in order to obtain the degree of Bachelor of Science at the Department of Quantum-Nanoscience, wich is a part of the Faculty of Applied Sciences at the Delft University of Technology.

Chapter 2

Theory

2.1 Quantum Transport using Non-Equilibrium Green's Functions

This section will follow the explanation of the excellent booklet *Non Equilibrium Green's Functions for Dummies: Introduction to the One Particle NEGF Equations* by Magnus Paulsson [10]. In this thesis the transport of electrons through a Helicene molecule connected to two gold contacts is considered. The left and right contact are both considered to be semi-infinite and connected to a reservoir of electrons with chemical potentials μ_L and μ_R. Starting form the time independent Schrödinger equation, the Hamiltonian is divided up into the contact Hamiltonians ($\hat{H}_{L,R}$ and $|\psi_{L,R}\rangle$) and a molecule Hamiltonian ($\hat{H}_m$ and $|\psi_m\rangle$). On a finite basis, the Time Independent Schrödinger equation then takes the form:

$$\begin{pmatrix} \hat{H}_L & \hat{\tau}_L & 0 \\ \hat{\tau}_L^\dagger & \hat{H}_m & \hat{\tau}_R^\dagger \\ 0 & \hat{\tau}_R & \hat{H}_R \end{pmatrix} \begin{pmatrix} |\psi_L\rangle \\ |\psi_m\rangle \\ |\psi_R\rangle \end{pmatrix} = E \begin{pmatrix} |\psi_L\rangle \\ |\psi_m\rangle \\ |\psi_R\rangle \end{pmatrix}. \tag{2.1}$$

Where $\hat{\tau}_{L,R}$ describes the interaction between the respective contact and the helicene molecule.

2.1.1 Green's Function

Because the system is not an isolated system anymore but connected to large reservoirs, diagnonalising the Hamiltonian would become a long and laborious process. That is, if it is possible at all. In these cases using Green's function $\hat{G}$ is often a faster and easier way to obtain information about quantum mechanical systems. Green's function is defined as:

$$(E\hat{I} - \hat{H})\hat{G}(E) = \hat{I}, \tag{2.2}$$

where $\hat{I}$ is the Identity Operator: $\hat{I}\left|\psi\right\rangle = \left|\psi\right\rangle$ for any $\left|\psi\right\rangle$ in the Hilbert space. The Green's function can be seen as the response of a quantum mechanical system to a constant in time perturbation $\left|p\right\rangle$. This can be seen by writing the Schrödinger equation for a constant perturbation:

$$\hat{H}\left|\psi\right\rangle = E\left|\psi\right\rangle + \left|p\right\rangle. \tag{2.3}$$

So that we can write:

$$\left|\psi\right\rangle = -(E\hat{I} - \hat{H})^{-1}\left|p\right\rangle = -\hat{G}(E)\left|p\right\rangle. \tag{2.4}$$

Two solutions can be obtained to this equation. These are an incoming wave, called the advanced solution, and an outgoing wave, called the retarded solution. The solutions are obtained using the advanced Green's function $\hat{G}^A = \hat{G}^\dagger$ and the retarded Green's function $\hat{G}^R = \hat{G}$ respectively.

In this thesis a capital $\hat{G}$ will be used to denote the Green's function of the entire system and its sub matrices. A lowercase $\hat{g}$ will be used to refer to the Green's functions associated with the isolated contacts or molecule. For example $\hat{g}_m(E) = (E\hat{I} - \hat{H}_m)^{-1}$.

2.1.2 Self Energy

It turns out that the Green's function restricted to the Hilbert space of the molecule $\hat{G}_m$ can be calculated efficiently. Using Equation 2.2 we can derive an expression for $\hat{G}_m$.

$$\begin{pmatrix} E\hat{I} - \hat{H}_L & -\hat{\tau}_L & 0 \\ -\hat{\tau}_L^\dagger & E\hat{I} - \hat{H}_m & -\hat{\tau}_R^\dagger \\ 0 & -\hat{\tau}_R & E\hat{I} - \hat{H}_R \end{pmatrix} \begin{pmatrix} \hat{G}_L & \hat{G}_{Lm} & \hat{G}_{LR} \\ \hat{G}_{mL} & \hat{G}_m & \hat{G}_{mR} \\ \hat{G}_{RL} & \hat{G}_{Rm} & \hat{G}_R \end{pmatrix} = \begin{pmatrix} \hat{I} & 0 & 0 \\ 0 & \hat{I} & 0 \\ 0 & 0 & \hat{I} \end{pmatrix} \tag{2.5}$$

The system of equations provided by the second column of Green's function has three unknowns and three equations. Therefore an expression for $\hat{G}_m$ can be found in terms of $E, \hat{H}_m, \hat{\tau}_L, \hat{\tau}_R, \hat{g}_L$ and $\hat{g}_R$.

$$\begin{aligned} (E - \hat{H}_L)\hat{G}_{Lm} - \hat{\tau}_L G_m &= 0 \\ -\hat{\tau}_L^\dagger \hat{G}_{Lm} + (E\hat{I} - \hat{H}_m)\hat{G}_m - \hat{\tau}_R^\dagger \hat{G}_{Rm} &= \hat{I} \\ -\hat{\tau}_R \hat{G}_m + (E\hat{I} - \hat{H}_R)\hat{G}_{Rm} &= 0 \end{aligned} \tag{2.6}$$

Using the first and last equation we can easily solve for $\hat{G}_{Lm}$ and $\hat{G}_{Rm}$.

$$\hat{G}_{Lm} = \hat{g}_L \hat{\tau}_L \hat{G}_m \tag{2.7}$$

$$\hat{G}_{Rm} = \hat{g}_R \hat{\tau}_R \hat{G}_m \tag{2.8}$$

Substitution in the second equations yields:

$$-\hat{\tau}_L^\dagger \hat{g}_L \hat{\tau}_L \hat{G}_m + (E\hat{I} - \hat{H}_m)\hat{G}_m - \hat{\tau}_R^\dagger \hat{g}_R \hat{\tau}_R \hat{G}_m = \hat{I}. \tag{2.9}$$

Now, define the self energies $\hat{\Sigma}$ as:

$$\hat{\Sigma}_{L,R} = -\hat{\tau}_{L,R}^\dagger \hat{g}_{L,R} \hat{\tau}_{L,R}. \tag{2.10}$$

Using this definition we can rewrite Equation 2.9 as:

$$\hat{G}_m = (E\hat{I} - \hat{H}_m - \hat{\Sigma}_L - \hat{\Sigma}_R)^{-1}. \tag{2.11}$$

When comparing Equation 2.11 to the definition of Green's function for the isolated molecule can say that the effect of the contacts is to add their respective self energy to the hamiltonian of the molecule. Thereby creating an effective Hamiltonian $\hat{H}_m^{\text{eff}} = \hat{H}_m + \hat{\Sigma}_L + \hat{\Sigma}_R$.

2.1.3 The Spectral Function

The spectral function $\hat{A}$ is an important operator which can be obtained from the Green's function since it yields the Density Of States (DOS). The spectral function is defined as:

$$\hat{A} = i(\hat{G}^R - \hat{G}^A) = i\text{Im}(\hat{G}), \tag{2.12}$$

where $|k\rangle$ are eigenvectors of G. By expanding the Green's function in its eigenbasis,

$$\hat{G} = \frac{1}{E\hat{I} - \hat{H}} = \sum_k \frac{|k\rangle \langle k|}{E - \epsilon_k}, \tag{2.13}$$

we can see that we can rewrite the spectral function as:

$$\hat{A} = 2\pi \sum_k \delta(E - E_k) |k\rangle \langle k| . \tag{2.14}$$

The Density of States can be obtained as follows from the spectral function:

$$DOS(E) = -\frac{1}{\pi} Tr \left[\hat{A}(E)\right]. \tag{2.15}$$

2.1.4 Single Particle Transport

First consider the isolated left contact. At the end of the contact waves at a certain energy will be totally reflected back into the contact. These solutions are denoted by $|\psi_{L,n}\rangle$. The n is a quantum number denoting different modes in the contact. All these solutions can be obtained using the spectral function of the isolated left contact $\hat{a}_L = i(\hat{g}_L^R - \hat{g}_L^A)$, since Equation 2.14 shows that $\hat{a}_L$ can give all the solutions to the Schrödinger equation of the isolated left contact [10].

Next, calculate the wave function of the whole system (the left contact, molecule and right contact) such that the solution coincides with $|\psi_{L,n}\rangle$ in the left contact. Note that the total response should be of the form $|\psi_{L,n}\rangle + |\psi^R\rangle$, where $|\psi^R\rangle$ is the retarded response of the entire system. Using this as an Ansatz and plugging it into the time independent Schrödinger equation gives:

$$(\hat{H}_L + \hat{\tau}_L + \hat{\tau}_L^\dagger + \hat{H}_m + \hat{\tau}_R^\dagger + \hat{\tau}_R + \hat{H}_R)(|\psi_{L,n}\rangle + |\psi^R\rangle) = E(|\psi_{L,n}\rangle + |\psi^R\rangle). \quad (2.16)$$

Solving for $|\psi^R\rangle$ yields:

$$|\psi^R\rangle = (E\hat{I} - \hat{H})^{-1}\hat{\tau}_L^\dagger |\psi_{L,n}\rangle = \hat{G}\hat{\tau}_L^\dagger |\psi_{L,n}\rangle, \quad (2.17)$$

where $\hat{H} = \hat{H}_L + \hat{\tau}_L + ... + \hat{H}_R$. So we could can view $|\psi^R\rangle$ as the response of the system to the perturbation $\hat{\tau}_L^\dagger |\psi_{L,n}\rangle$. By choosing to use the retarded response the only part of the wave that is travelling towards the device is the incoming wave $|\psi_{L,n}\rangle$ we can write expressions for the wave function of the molecule $|\psi_m\rangle$ and the contact wave functions $|\psi_{L,R}\rangle$:

$$|\psi_m\rangle = \hat{G}_m\hat{\tau}_L^\dagger |\psi_{L,n}\rangle. \quad (2.18)$$

Using the third row of Equation 2.1, an expression for the wave-function in the contacts can be easily derived:

$$\hat{H}_R |\psi_R\rangle + \hat{\tau}_R |\psi_m\rangle = E |\psi_R\rangle \rightarrow |\psi_R\rangle = \hat{g}_R\hat{\tau}_R |\psi_m\rangle. \quad (2.19)$$

Substituting Equation 2.18 yields an expression for $|\psi_R\rangle$ in terms of $|\psi_{L,n}\rangle$:

$$|\psi_R\rangle = \hat{g}_R\hat{\tau}_R\hat{G}_m\hat{\tau}_L^\dagger |\psi_{L,n}\rangle. \quad (2.20)$$

The wave function of the left contact is a bit more complicated, since we need to also consider the incoming wave:

$$|\psi_L\rangle = |\psi_{L,n}\rangle + \hat{g}_L\hat{\tau}_L |\psi_m\rangle = (\hat{I} + \hat{g}_L\hat{\tau}_L\hat{G}_m\hat{\tau}_L^\dagger) |\psi_{L,n}\rangle. \quad (2.21)$$

Using the expressions found for these wave functions, our goal can be achieved: Calculating the charge density and the current through the molecule.

Charge Density

The definition of the Charge Density matrix is:

$$\hat{\rho} = \sum_k f(E_k, \mu) \left|\psi_k\right\rangle \left\langle\psi_k\right| , \tag{2.22}$$

where $f(E_k, \mu)$ are the occupation numbers of the electrons. Since electrons are fermions, in this case $f(E_k, \mu)$ is the Fermi-Dirac distribution:

$$f(E_k, \mu) = \frac{1}{1 + e^{\beta(E_k - \mu)}}, \tag{2.23}$$

where $\beta = \frac{1}{k_B T}$, k_B is the Boltzmann constant and T is the temperature. In this case μ and T are properties of the reservoir that is injecting the electrons into the system. Using the definition of $\hat{\rho}$, $f(E_k, \mu)$ and Equation 2.18 we can write for the contribution of the left contact:

$$\hat{\rho}_{m,L} = \int_{-\infty}^{\infty} \sum_k f(E, \mu_L) \delta(E - E_k) \hat{G}_m \hat{\tau}_L^\dagger \left|\psi_{L,k}\right\rangle \left\langle\psi_{L,k}\right| \hat{\tau}_L \hat{G}_m^\dagger dE. \tag{2.24}$$

This can be rewritten as, using Equation 2.14:

$$\hat{\rho}_{m,L} = \frac{1}{2\pi} \int_{-\infty}^{\infty} f(E, \mu_L) \hat{G}_m \hat{\tau}_L^\dagger \hat{a}_L \hat{\tau}_L \hat{G}_m^\dagger dE. \tag{2.25}$$

Now defining $\hat{\Gamma}_i = \hat{\tau}_i^\dagger \hat{a}_i \hat{\tau}_i = i(\Sigma_i - \Sigma_i^\dagger)$ yields:

$$\hat{\rho}_{m,L} = \frac{1}{2\pi} \int_{-\infty}^{\infty} f(E, \mu_L) \hat{G}_m \hat{\Gamma}_L \hat{G}_m^\dagger dE. \tag{2.26}$$

Summing the result of both the contacts and multiplying by two for spin yields the following equation:

$$\hat{\rho}_m = \frac{2}{2\pi} \int_{-\infty}^{\infty} \left(f(E, \mu_L) \hat{G}_m \hat{\Gamma}_L \hat{G}_m^\dagger + f(E, \mu_R) \hat{G}_m \hat{\Gamma}_R \hat{G}_m^\dagger \right) dE, \tag{2.27}$$

where μ_L and μ_R are the chemical potentials in the Left and Right contacts.

Current

Before the electrical current can be calculated, the current of the wave function of the electrons has to be calculated first. This can be done by noticing that, during a steady state current, the probability to find an electron in the system is conserved:

$$\frac{\partial}{\partial t} \sum_i |\psi_i|^2 = 0, \tag{2.28}$$

where the sum runs over the molecule Hilbert space. Working this out via the product rule for derivatives the following result is obtained:

$$\begin{aligned}&\frac{i}{\hbar}\left[\langle\psi_L|\,\hat{\tau}_L\,|\psi_m\rangle-\langle\psi_m|\,\hat{\tau}_L^\dagger\,|\psi_L\rangle\right]+\\&\frac{i}{\hbar}\left[\langle\psi_R|\,\hat{\tau}_R\,|\psi_m\rangle-\langle\psi_m|\,\hat{\tau}_R^\dagger\,|\psi_R\rangle\right]=0.\end{aligned}\tag{2.29}$$

It seems that the incoming probability currents from the left and right contacts should be equal but opposite. Thus if the electrical current is defined as:

$$i_j=\frac{ie}{\hbar}\left[\langle\psi_j|\,\hat{\tau}_j\,|\psi_m\rangle-\langle\psi_m|\,\hat{\tau}_j^\dagger\,|\psi_j\rangle\right],\tag{2.30}$$

where $j\in\{L,R\}$ and e is the electron charge. The total electrical current through the system can be found in a similar way as to an expression for the charge matrix was found. Now rewriting Equation 2.30 using equations 2.18 and 2.20 we obtain:

$$i_{LR}=-\frac{e}{\hbar}\langle\psi_{1,n}|\,\hat{\tau}_L\hat{G}_m^\dagger\hat{\Gamma}_R\hat{G}_m\hat{\tau}_L^\dagger\,|\psi_{1,n}\rangle\,.\tag{2.31}$$

Summing over all the modes n in the contact and noting that the energy levels are filled according to the Fermi-Dirac Distribution yields the following expression for the current from the left to the right contact:

$$I_{LR}=\frac{e}{\pi\hbar}\int_{-\infty}^{\infty}f(E,\mu_L)Tr\left[\hat{G}_m^\dagger\hat{\Gamma}_R\hat{G}_m\hat{\Gamma}_L\right]dE.\tag{2.32}$$

The total current $I=I_{LR}-I_{RL}$ then becomes:

$$I=-\frac{e}{\pi\hbar}\int_{-\infty}^{\infty}\left(f(E,\mu_L)-f(E,\mu_R)\right)Tr\left[\hat{G}_m^\dagger\hat{\Gamma}_R\hat{G}_m\hat{\Gamma}_L\right]dE,\tag{2.33}$$

which is the Landauer formula for current. Note that:

$$T=Tr\left[\hat{G}_m^\dagger\hat{\Gamma}_R\hat{G}_m\hat{\Gamma}_L\right]\tag{2.34}$$

is called the transmission of the molecule. This is the Meir-Wingreen formula and this what will be used in Chapter 3 to calculate the transmissions.

2.2 Self Consistency Methods

The explanation in this section follows the explanations in the book *Computational Physics* by Jos Thijssen [16] in chapters 4 and 5.

For a system of N electrons and K nuclei the Hamiltonian reads:

$$\hat{H} = \sum_{i=1}^{N} \frac{\hat{p}_i^2}{2m} + \sum_{n=1}^{K} \frac{\hat{P}_n^2}{M_n} + \frac{1}{4\pi\epsilon_0}\frac{1}{2} \sum_{i,j=1;i\neq j}^{N} \frac{e^2}{|\boldsymbol{r}_i - \boldsymbol{r}_j|} - \\ \frac{1}{4\pi\epsilon_0} \sum_{n=1}^{K}\sum_{i=1}^{N} \frac{Z_n e^2}{|\boldsymbol{r}_i - \boldsymbol{R}_n|} + \frac{1}{4\pi\epsilon_0}\frac{1}{2} \sum_{n,n'=1;n\neq n'}^{K} \frac{Z_n Z_{n'} e^2}{|\boldsymbol{R}_n - \boldsymbol{R}_{n'}|}, \quad (2.35)$$

where uppercase letters are used to denote properties of the nuclei and lowercase letters are used for the electrons. The first and second term account for the kinetic energy of the electrons and nuclei respectively. The third, fourth and fifth terms describe the electrostatic interaction between the electrons themselves, the electrons and the nuclei and the nuclei themselves respectively.

This Hamiltonian is unsolvable for all but the smallest systems, thus approximations are in order. A first approximation to be made is the so-called Born-Oppenheimer approximation in which the nuclei are considered to have fixed positions. That this approximation is valid can be seen by realising that the nuclei are a couple of orders of magnitude heavier than the electrons. A single proton is already almost 2,000 times heavier than an electron. Thus the Born-Oppenheimer approximation seems to make sense.

The Hamiltonian found after using the Born-Oppenheimer approximation is:

$$\hat{H}_{BO} = \sum_{i=1}^{N} \frac{\hat{p}_i^2}{2m} + \frac{1}{4\pi\epsilon_0}\frac{1}{2} \sum_{i,j=1;i\neq j}^{N} \frac{e^2}{|\boldsymbol{r}_i - \boldsymbol{r}_j|} - \frac{1}{4\pi\epsilon_0} \sum_{i=1}^{N}\sum_{n=1}^{K} \frac{Z_n e^2}{|\boldsymbol{r}_i - \boldsymbol{R}_n|}. \quad (2.36)$$

Because in this approximation the electrons are still interacting with each other, the problem remains nearly impossible to solve for systems of over a handful of particles. If the second term, which describes the electrostatic interaction between electrons, would not be there the problem would reduces to a set of single particle Hamiltonians.

Briefly forgetting about the second term, uncouple the problem into a set of Independent Particle Hamiltonians, defined as:

$$\hat{H}_{\mathrm{IP}} = \sum_{i=1}^{N} \left[\frac{\hat{p_i}^2}{2m} + \hat{V}(\boldsymbol{r}_i) \right]. \quad (2.37)$$

Now, the eigenfunctions of this Hamiltonian can be found approximately in an iterative fashion. The difficulty of the problem resides in determining the $\hat{V}$s. In any case $\hat{V}(\boldsymbol{r}_i)$ depends on the locations of the nuclei. $\hat{V}$ also depends on the current location but also on other locations, meaning it is non-local, on the wave function $|\psi\rangle$ it is acting. $\hat{V}$ also depends on the eigenstates $|\psi_j\rangle$ of the independent particle Hamiltonian, therefore the independent particle Hamiltonian has to be solved iteratively.

2.2.1 Hartree-Fock Theory

In Hartree Fock Theory (HFT) the wave functions are restricted to be Slater determinants:

$$\Psi_{AS}(\boldsymbol{x_1}, ..., \boldsymbol{x_N}) = \frac{1}{\sqrt{N!}} \begin{vmatrix} \psi_1(\boldsymbol{x_1}) & \cdots & \psi_N(\boldsymbol{x_1}) \\ \vdots & \ddots & \vdots \\ \psi_1(\boldsymbol{x_N}) & \cdots & \psi_N(\boldsymbol{x_N}) \end{vmatrix}. \tag{2.38}$$

These Determinants per definition take care of the anti-symmetry requirement for fermionic wave functions. Using Equation 2.38 with the Born-Oppenheimer approximation yields the following Schrödinger Equation:

$$\begin{aligned} \hat{\mathcal{F}}\psi_k = & \left[-\frac{1}{2}\nabla^2 - \sum_{n=1}^{K} \frac{Z_n}{|\boldsymbol{r} - \boldsymbol{R_n}|} \right] \psi_k(\boldsymbol{x}) + \\ & \sum_{l=1}^{N} \int |\psi_l(\boldsymbol{x'})|^2 \frac{1}{|\boldsymbol{r} - \boldsymbol{r'}|} \psi_k(\boldsymbol{x}) dx' - \\ & \sum_{l=1}^{N} \int \psi_l(\boldsymbol{x'})^* \frac{1}{|\boldsymbol{r} - \boldsymbol{r'}|} \psi_k(\boldsymbol{x'}) \psi_l(\boldsymbol{x}) dx'. \end{aligned} \tag{2.39}$$

This is called the Hartree-Fock equation and $\hat{\mathcal{F}}$ is called the Fock operator. The first term of the HF equation describes the kinetic energy of the electrons, the second term describes the electrostatic interaction between the electrons and the nuclei, the third term describes the electrostatic interaction between the electrons themselves and the fourth term takes care of the anti-symmetry requirement by interchanging the spin terms and taking the whole term to be negative.

A solution for the wave functions $|\psi_{k,0}\rangle$ can now be found by taking a first guess at $|\psi_{k,0}\rangle$ and filling them into Equation 2.39. This yields a new set of orbitals $|\psi_{k,1}\rangle$ which in their turn are filled back into the Hartree-Fock equation which yields again a new set of orbitals. This is repeated until convergence is reached.

2.2.2 Density Functional Theory

In DFT electron orbitals are solutions to a Schrödinger equation which depends on electron density instead on individual electron orbitals. An effective independent particle Hamiltonian is used, which gives rise to the following Schrödinger equation:

$$\left[-\frac{1}{2}\nabla^2 - \sum_{n=1}^{K}\frac{1}{|\boldsymbol{r}-\boldsymbol{r}'|} + \int n(\boldsymbol{r}')\frac{1}{|\boldsymbol{r}-\boldsymbol{r}'|}d^3r' + V_{XC}[n](\boldsymbol{r})\right]\psi_k(\boldsymbol{r}) = \epsilon_k\psi_k(\boldsymbol{r}). \tag{2.40}$$

The first three terms are identical to Hartree-Fock theory, but the fourth term is different. This term contains all the many-body effects and is called the exchange correlation potential. According to Density Functional Theory an exchange correlation potential exists which yields the exact ground state energy and electron density. However, this form is not known so, again, we will have to make do with a number of approximations.
The solution of the DFT Schrödinger equation must be consistent with the electron density $n(\boldsymbol{r})$, which is defined as:

$$n(\boldsymbol{r}) = \sum_{k=1}^{N}|\psi_k(\boldsymbol{r})|^2, \tag{2.41}$$

where N is again the total number of electrons. The total energy E is then given by:

$$E = \sum_{k=1}^{N}\epsilon_k - \frac{1}{2}\int\int n(\boldsymbol{r})\frac{1}{|\boldsymbol{r}-\boldsymbol{r}'|}n(\boldsymbol{r}')d^3r d^3r' + E_{XC}[n] - \int V_{XC}[n](\boldsymbol{r})n(\boldsymbol{r})d^3r, \tag{2.42}$$

where ϵ_k are the eigenvalues of the DFT Schrödinger equation and E_{XC} is the exchange correlation energy, which is related to the exchange correlation potential via:

$$V_{XC}[n](\boldsymbol{r}) = \frac{\delta}{\delta n(\boldsymbol{r})}E_{XC}[n]. \tag{2.43}$$

Furthermore, the wave functions $|\psi_k\rangle$ have no individual meaning other than to construct the electron density. In order to find the wave function, Equation 2.40 and Equation 2.41 have to be solved iteratively in a self consistency loop. DFT is in principle an exact method, but because the exact form of $V_{XC}[n]$ is unknown, the approximations discussed earlier have to be used. $V_{XC}[n]$ is a functional derivative of $E_{XC}[n]$ which is a functional of $n(\boldsymbol{r})$. For a homogeneous electron gas, the exchange correlation energy only depends on the local electron density. For a nonhomogeneous system $V_{XC}[n](\boldsymbol{r})$ not only depends on just the local electron density, but also on the variation of $n(\boldsymbol{r})$ close to $\boldsymbol{r}$:

$$V_{XC}[n](\boldsymbol{r}) = V_{XC}[n(\boldsymbol{r}), \nabla n(\boldsymbol{r}), \nabla(\nabla n(\boldsymbol{r})), ...]. \tag{2.44}$$

The variations in $n(\boldsymbol{r})$ make calculations significantly slower. Thus often the Ansatz is made that $V_{XC}[n]$ only depends on the local electron density. This is called the local density approximation (LDA).

$$E_{XC}[n] = \int \epsilon_{XC}[n(\boldsymbol{r})]n(\boldsymbol{r})d^3r, \tag{2.45}$$

where $\epsilon_{XC}[n]$ is the exchange correlation energy per particle of an homogeneous electron gas at density $n(\boldsymbol{r})$. The local density approximation is exact for homogeneous electron gasses.

2.3 Spin-Orbit coupling

In the Bohr model of the atom, when an electron is orbiting the nucleus of an atom the electron is held in place by the electric field $\boldsymbol{E}$ emitted by the nucleus. However in the reference frame of the electron it seems as though the nucleus is orbiting around the electron in a magnetic field $\boldsymbol{B}$. According to relativity this magnetic field takes the value in classical notation [5]:

$$\boldsymbol{B} = -\frac{\boldsymbol{v} \times \boldsymbol{E}}{c^2}, \tag{2.46}$$

where $\boldsymbol{v}$ is the velocity of the electron around the nucleus and c is the speed of light in a vacuum. Assuming that we are in the non-relativistic limit for the nucleus, thus the Lorentz factor $\gamma \approx 1$, it can also be seen that $\boldsymbol{E}$ must always point radially. That is, $\boldsymbol{E} = \left|\frac{E}{r}\right| \boldsymbol{r}$ where $\boldsymbol{r}$ is the radial position of the electron to the nucleus, and that the momentum of the electron is given by $\boldsymbol{p} = m_e\boldsymbol{v}$. Thus rewriting Equation 2.46 yields:

$$\boldsymbol{B} = \frac{\boldsymbol{r} \times \boldsymbol{p}}{m_e c}\left|\frac{E}{r}\right|. \tag{2.47}$$

From electrostatics it is a known fact that $\boldsymbol{E} = -\nabla V$, where V is the electrostatic potential in the vicinity of the nucleus. From the condition that $\boldsymbol{E}$ always points radially, it is found that V can only depend on r.

$$|E| = \frac{dV}{dr} = \frac{1}{e}\frac{dU}{dr}, \tag{2.48}$$

where $U = eV$ is the potential energy of the electron in the nuclear electric field and where e is the charge of the electron.

In classical mechanics the angular momentum of a particle is found by $\boldsymbol{L} = \boldsymbol{r} \times \boldsymbol{p}$. Thus rewriting Equation 2.47 further, switching to Dirac notation where $\boldsymbol{B}$ and $\boldsymbol{L}$ are vectors of operators:

$$\hat{\boldsymbol{B}} = \frac{1}{m_e e c^2} \frac{1}{r} \frac{dU}{dr} \hat{\boldsymbol{L}}. \tag{2.49}$$

This shows that the magnetic field the electron feels when orbiting around the nucleus is parallel to the angular momentum vector of the electron.
Due to $\hat{\boldsymbol{B}}$ the electron will feel two effects that affect its Hamiltonian $\hat{H}_0$. The spin vector $\hat{\boldsymbol{S}}$ will start to precess around the field lines of $\boldsymbol{B}$ and the intrinsic magnetic moment $\hat{\boldsymbol{\mu}}_s$ due to the spin of the electron will interact with the magnetic field. These effects are called Thomas precession and the Larmor interaction and describe the spin-orbit interaction of the electron. Thus the full Hamiltonian that governs the movement of the electron is:

$$\hat{H} = \hat{H}_0 + \Delta\hat{H} = \hat{H}_0 + \Delta\hat{H}_L + \Delta\hat{H}_T. \tag{2.50}$$

From Equation 2.50 it can be seen that the spin-orbit interaction perturbs the "original" Hamiltonian that governs the electron. Qualitatively this results in the splitting of energy levels.

Starting with the Larmor interaction. The contribution to the Hamiltonian by the Larmor interaction is given by the energy of a magnetic dipole moment in a magnetic field:

$$\Delta\hat{H}_T = -\hat{\boldsymbol{\mu}}_s \cdot \hat{\boldsymbol{B}}. \tag{2.51}$$

The magnetic dipole moment of the electron is given by:

$$\hat{\boldsymbol{\mu}}_s = -\frac{g_s \mu_B}{\hbar} \hat{\boldsymbol{S}}, \tag{2.52}$$

where $\hat{\boldsymbol{S}} = \hat{S}_x \boldsymbol{x} + \hat{S}_y \boldsymbol{y} + \hat{S}_z \boldsymbol{z}$ is the spin angular momentum vector, μ_B is the Bohr Magneton and $g_s \approx 2$ is the electron spin g-factor. Substituting Equation 2.52 and Equation 2.49 into Equation 2.51, it is found that:

$$\Delta\hat{H}_L = \frac{2\mu_B}{\hbar m_e e c^2} \frac{1}{r} \frac{dU}{dr} \left(\hat{\boldsymbol{S}} \cdot \hat{\boldsymbol{L}}\right). \tag{2.53}$$

The energy contribution of Thomas precession is given by:

$$\Delta\hat{H}_T = \hat{\boldsymbol{\Omega}}_T \cdot \hat{\boldsymbol{S}}, \tag{2.54}$$

where $\hat{\boldsymbol{\Omega}}_T$ is the Thomas precession rate, which is related to the angular velocity of the electron by $\hat{\boldsymbol{\Omega}}_T = \hat{\boldsymbol{\omega}}(\gamma - 1)$. When Equation 2.54 is approximated to first order in $\left(\frac{v}{c}\right)^2$ it is found that:

$$\Delta\hat{H}_T = -\frac{\mu_B}{\hbar m_e e c^2} \frac{1}{r} \frac{dU}{dr} \left(\hat{\boldsymbol{S}} \cdot \hat{\boldsymbol{L}}\right). \tag{2.55}$$

Thus filling the results of $\Delta\hat{H}_L$ and $\Delta\hat{H}_T$ into Equation 2.50 we find that $\hat{H}_0$ is perturbed by the spin-orbit interaction by:

$$\Delta\hat{H} = \Delta\hat{H}_L + \Delta\hat{H}_T = \frac{\mu_b}{\hbar m_e e c^2}\frac{1}{r}\frac{dU}{dr}\left(\hat{\boldsymbol{L}}\cdot\hat{\boldsymbol{S}}\right). \tag{2.56}$$

Because $\hat{\boldsymbol{L}}$ and $\hat{\boldsymbol{S}}$ need to be considered together in the Hamiltonian, they are no longer conserved quantities. Therefore the total angular momentum $\hat{\boldsymbol{J}}$ is introduced:

$$\hat{\boldsymbol{J}} = \hat{\boldsymbol{L}} + \hat{\boldsymbol{S}}. \tag{2.57}$$

It can then be easily seen that, because $\hat{\boldsymbol{L}}$ and $\hat{\boldsymbol{S}}$ commute:

$$\hat{J}^2 = \hat{L}^2 + \hat{S}^2 + 2\hat{\boldsymbol{L}}\cdot\hat{\boldsymbol{S}}. \tag{2.58}$$

Rewriting this to find an expression for $\hat{\boldsymbol{L}}\cdot\hat{\boldsymbol{S}}$:

$$\hat{\boldsymbol{L}}\cdot\hat{\boldsymbol{S}} = \frac{1}{2}\left(\hat{J}^2 - \hat{L}^2 - \hat{S}^2\right). \tag{2.59}$$

Thus the expectation energy of the energy added by $\Delta\hat{H}$ can be found via:

$$\langle\Delta E\rangle = \langle njlsm_j|\,\Delta\hat{H}\,|njlsm_j\rangle = \frac{C}{2}\left[j(j-1) + l(l-1) + s(s-1)\right]. \tag{2.60}$$

Where C contains all the constants of Equation 2.56.

Chapter 3

Method

In this chapter the methods behind a transport calculation through a thiolated 4-Helicene molecule sandwiched between two gold contacts is calculated. This is done using the Amsterdam Density Functional (ADF) package supplied by the Software for Chemistry and Materials (SCM) [1] [14] [2]. In the first section, the geometry of the Helicene molecule will be determined in three ways according to the methods used in [15]. In the second section the methods behind the actual transport calculations will be presented. The legacy method used by ADF [13] and the newly implemented method developed by Marnix Rebergen in [11] will be presented separately. They will be called the Single Green Method and the Double Green Method respectively. After being presented, they will be compared and their differences will be discussed.

3.1 Geometry Optimisation

Before any kind of transport calculation can be executed, the Hamiltonian of the molecule over which the transport calculation is preformed must be known. To that effect the shape of the molecule must be known. The entire system consists of three parts. From left to right the system consists of: the left contact, the extended molecule and the right contact. The extended molecule can be seen in Figure 3.1. The extended molecule is a compound system consisting of the 4-Helicene molecule thiol bonded to two gold leads, these leads are principal layers of gold. The gold atoms on one side of a principal layer do not influence the gold atoms in the next principal layer on the other side of the layer, for gold a principal layer is three atoms thick.

The contacts are constructed from a trapezoidal crystal of gold containing three principal layers, these principal layers are three atoms wide, high

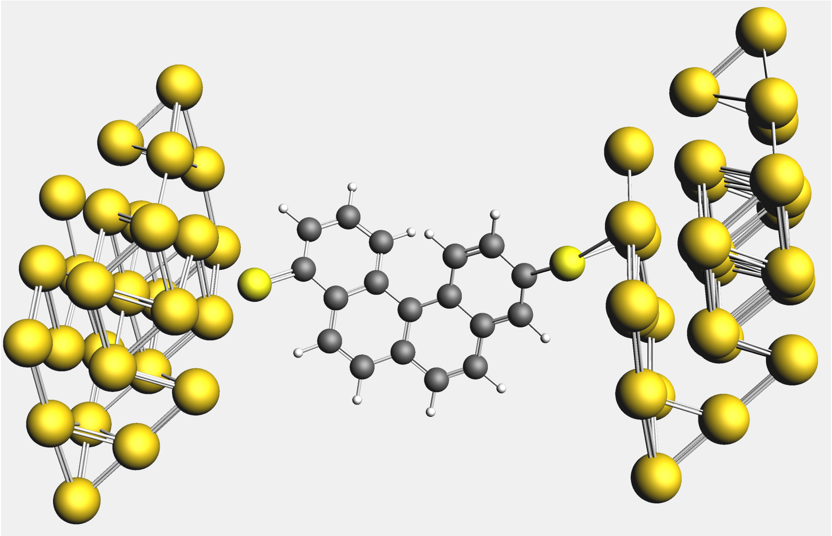

Figure 3.1: The extended molecule used in the Transport and Density of States calculations.

and deep. By doing this, the Hamiltonian on the interfaces of the principal layers approximate a bulk Hamiltonian quite well. This can be seen in Figure 3.2. Therefore a self consistent Density Functional Theory (DFT) calculation will be done first over the entire crystal using the Zero Order Regular Approximation (ZORA) to the Dirac equation using ADF. ZORA accounts for relativistic effects such as spin-orbit coupling. After that the self energy of the right contact will be calculated on the interface between the green and blue principal layers and the self energy of the left contact will be calculated on the interface between the red and green contact. Thus the contacts are effectively build up as two consecutive principal layers of gold.

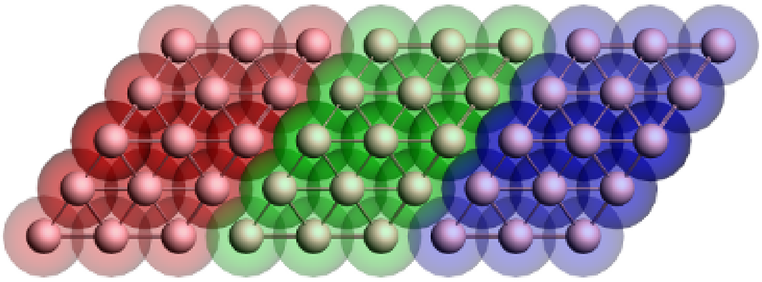

Figure 3.2: Three principal layers of gold. Because the atoms in a principal layer do not influence the atoms two layers apart, the Hamiltonian of the central layer resembles a bulk Hamiltonian. [12]

In the extended molecule the 4-Helicene molecule will interact with the gold leads and change its geometry accordingly. The gold atoms in the leads are also influenced by the Helicene and will also adapt their positions. This is accounted for by a geometry optimisation procedure using ADF. This will be done in three different ways according to the methods presented in the Bachelor Thesis by Annick Teepe [15] on which this thesis directly builds. All three methods had an initial geometry optimisation preceding them. The three methods are:

- No further optimisation is done.
- A second geometry optimisation procedure is executed where the y and z coordinates of the gold contacts were kept fixed, so the gold atoms could only move in the x direction. This geometry will no be referred to as the first optimised geometry
- A second geometry optimisation procedure is executed where the gold contacts are kept completely fixed in the positions after the first geometry optimisation. This geometry will now be referred to as the second optimised geometry.

3.2 Transport and Density of States Calculations

When calculating the transport of electrons through the Helicene molecule the Landauer Equation (Equation 2.33) must be solved over the entire system. To be able to solve this equation, some preparations have to be made. First, self-consistent Density Functional Theory calculations are preformed by ADF over each geometry using the ZORA Dirac Equation. The DFT run yields a set of spatial orbitals $\phi_k^i(\vec{r})$ the electron density $n(\vec{r})$ and the ground state energy E for each of the fragments of the extended molecule using Equations 2.40 and 2.41. The spatial orbitals for each fragment can expressed in a basis of Slater Type Orbitals $\chi_j(\vec{r})$, see Equation 2.38:

$$\phi_k^i(\vec{r}) = \sum_j A_j^{i,k} \chi_j(\vec{r}), \tag{3.1}$$

where i denotes the fragment: L for the left contact, R for the right contact and m for the molecule. Then these orbitals are used as a basis for a spin unrestricted ZORA-DFT run over the entire extended molecule. This results in a set of spin-orbitals, a product of spatial orbitals and spin states A and B:

$$\psi_k(\vec{r},s) = \sum_{i,j} C^A_{k,j}\phi^i_j(\vec{r})\left|A\right\rangle + \sum_{i,j} C^B_{k,j}\phi^i_j(\vec{r})\left|B\right\rangle . \tag{3.2}$$

Second, the Green's function for each geometry of the extended molecule $\hat{G}_m$ must be calculated via Equation 2.11. For this the molecule's Hamiltonian $\hat{H}_m$ must be known and the self energies $\hat{\Sigma}_i$ of the contacts must be calculated via Equation 2.10. The Hamiltonian of the molecule is defined as the Fock matrix $\hat{F}_m$. The Fock matrix is calculated via:

$$\hat{F} = \hat{S}\hat{C}\hat{E}\hat{C}^\dagger\hat{S}, \tag{3.3}$$

where $\hat{C}$ is a matrix where each column is an orbital defined in equation 3.2, $\hat{S} = (\hat{C}\hat{C}^\dagger)^{-1}$ is the overlap matrix between the valence orbitals of the molecule, $\hat{E}$ is the matrix containing the energy points defined in the input. Thus Equation 2.11 can now be rewritten as:

$$\hat{G}_m(E) = \left(E\hat{S} - \hat{F}_m - \hat{\Sigma}_l - \hat{\Sigma}_r\right)^{-1}, \tag{3.4}$$

where in this case E is not a matrix, but the scalar input value of Green's function. As described in the previous section, using Figure 3.2, the self energy of the right contact $\hat{\Sigma}_r$ is calculated on the interface between the green and blue principal layers and the self energy of the left contact $\hat{\Sigma}_l$ is calculated on the interface between the red and green principal layers. Then the Gamma matrices $\hat{\Gamma}$ can be calculated via $\hat{\Gamma}_i = i(\hat{\Sigma}_i - \hat{\Sigma}_i^\dagger)$.

3.2.1 The Single Green Method

This is the Non-Self-Consistent Green's function calculation provided by ADF, created by J. Seldenthuijs [13]. In the way it is currently implemented in ADF this method does not allow for calculations using ZORA-DFT including spin-orbit interactions. In a spin unrestricted Single Green calculation ADF essentially preforms the same calculation twice for both spin directions, which will be called A and B. In this case two $\hat{C}$ matrices are defined. $\hat{C}_A$ contains the coefficients $C^A_{k,j}$ from Equation 3.2 as entries and $\hat{C}_B$ contains the coefficients $C^B_{k,j}$ as entries. Thus two Green's functions are defined $\hat{G}_{m,A}$ and $\hat{G}_{m,B}$, which yields two Transmissions T_A and T_B via:

$$T_i = \mathrm{Tr}\left[\hat{G}^\dagger_{m,i}\hat{\Gamma}_R\hat{G}_{m,i}\hat{\Gamma}_L\right]. \tag{3.5}$$

Two Densities of States, DOS_A and DOS_B are also obtained via Equation 2.15:

$$DOS_i = \frac{1}{\pi}\text{Tr}\left[Im\left(\hat{G}_{m,i}\right)\hat{S}_i\right], \tag{3.6}$$

where i is either A or B. From these equations it can be seen that spin polarisation would only occur when there is a difference in $\hat{G}_{m,A}$ and $\hat{G}_{m,B}$, which translates through equation 3.4 into a difference in the Fock matrices $\hat{F}_{m,A}$ and $\hat{F}_{m,B}$. Now looking at equation 3.3 it can be seen that (since $\hat{E}$ is the same for both spin directions, it was defined in the input) spin polarisation can only occur when the valence orbitals are different for the spin directions. Since Helicene is considered, an organic molecule with negligible spin-orbit interaction for the outer orbitals, this model will not predict any spin polarisation without the presence of a magnetic field.

3.2.2 The Double Green Method

This method was proposed by Marnix Rebergen in his Masters thesis [11]. This method is a more direct approach to the problem, since the calculation is not divided up into two separate calculations for both spin directions, but one large calculation. In this case $\hat{C}$ is a $2N$ x k matrix, where the first N rows contain the $C^A_{k,j}$ coefficients and the last N rows contain the $C^B_{k,j}$ coefficients. Thus $\hat{S}$ is now a $2N$ x $2N$ matrix which is not necessarily block-diagonal, since there might be some overlap between spin-A orbitals and spin-B orbitals. It then follows that $\hat{G}_m$ might not be block diagonal as well and thus electrons of different spin might be interaction with each-other. The transmission must now also account for spin flip processes. Therefore, the transmission of spin-A and spin-B must now be calculated as:

$$\begin{aligned} T_A &= t_{AA} + t_{BA} \\ T_B &= t_{BB} + t_{AB}, \end{aligned} \tag{3.7}$$

where t_{ii} is the transmission of spin-i to spin-i and t_{ij} is the transmission of spin-i to spin-j. Now the bookkeeping starts kicking into gear. The four spin-to-spin transmissions are calculated via:

$$\begin{aligned} t_{AA} &= \text{Tr}\left[\hat{G}^\dagger_{AA}\hat{\Gamma}_R\hat{G}_{AA}\hat{\Gamma}_L\right] \\ t_{AB} &= \text{Tr}\left[\hat{G}^\dagger_{AB}\hat{\Gamma}_R\hat{G}_{AB}\hat{\Gamma}_L\right] \\ t_{BA} &= \text{Tr}\left[\hat{G}^\dagger_{BA}\hat{\Gamma}_R\hat{G}_{BA}\hat{\Gamma}_L\right] \\ t_{BB} &= \text{Tr}\left[\hat{G}^\dagger_{BB}\hat{\Gamma}_R\hat{G}_{BB}\hat{\Gamma}_L\right], \end{aligned} \tag{3.8}$$

where $\hat{G}_{ij}$ with $i, j \in \{A, B\}$ is a sub-matrix of the full Green's function $\hat{G}_m$ associated with t_{ij}. Because the spins are allowed to interact with each other in this method, spin polarisation could occur when one spin flip is stronger than the other spin flip term.

The DOS can now be calculated by:

$$\begin{aligned} DOS_A &= \tfrac{1}{\pi}\mathrm{Tr}[Im(\hat{G}_A)] \\ DOS_B &= \tfrac{1}{\pi}\mathrm{Tr}[Im(\hat{G}_B)], \end{aligned} \tag{3.9}$$

where $\hat{G}_i$ are the block-diagonal sub-matrices of the full Green's function equivalent to the $\hat{G}_A$ and $\hat{G}_B$ of the Single Green method.

Chapter 4

Results

4.1 The Single Green Method

The results for the Transmission and Density of States calculations using the Single Green Method for all three geometries are presented in figures 4.1, 4.2 and 4.3

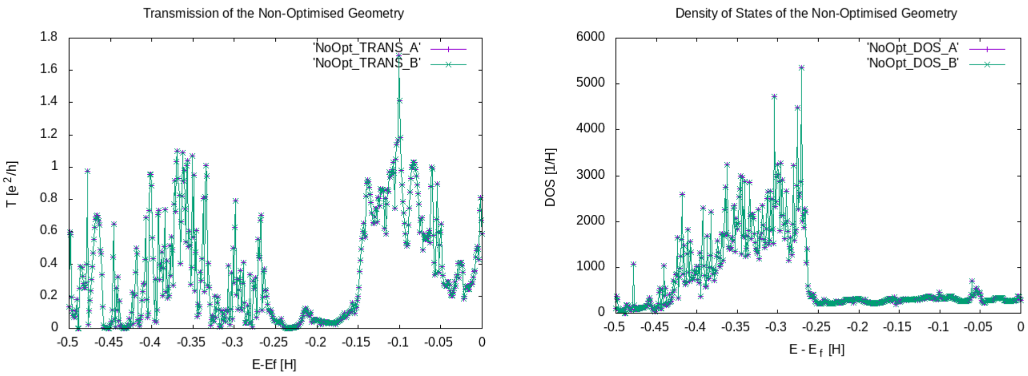

(a) Transmission of the non-optimised geometry.

(b) Density of States of the non-optimised geometry.

Figure 4.1: Transmission and Density of States of the Non-Optimised geometry using the Single Green Method. The purple line indicates the spin-A and the cyan line indicates the spin-B.

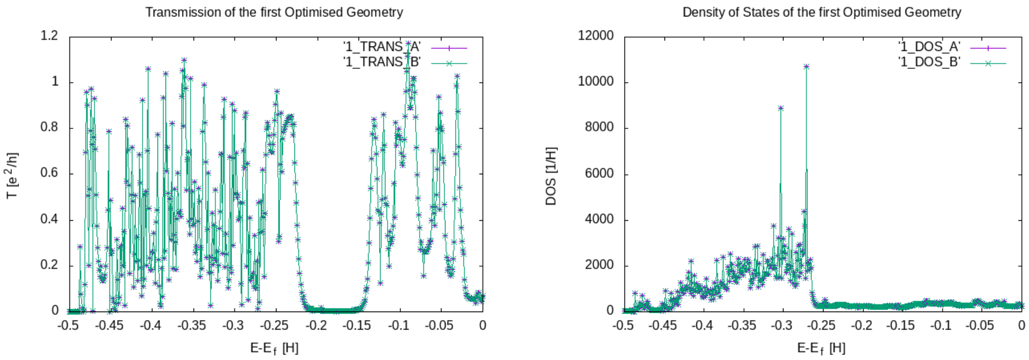

(a) Transmission of the first optimised geometry.

(b) Density of States of the first optimised geometry.

Figure 4.2: Transmission and Density of States of the First Optimised geometry using the Single Green Method. The purple line indicates the spin-A and the cyan line indicates the spin-B.

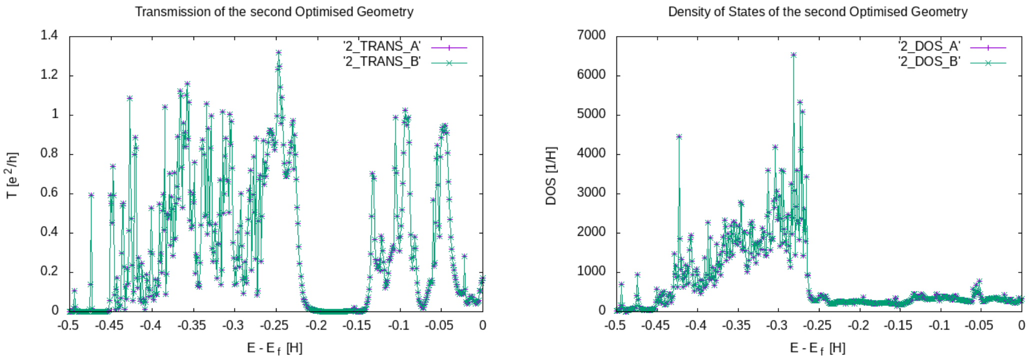

(a) Transmission of the second optimised geometry.

(b) Density of States of the second optimised geometry.

Figure 4.3: Transmission and Density of States of the Second Optimised geometry using the Single Green Method. The purple line indicates the spin-A and the cyan line indicates the spin-B.

As can be seen clearly no spin polarisation whatsoever occurs in the Transmission and DOS energy spectra when using the Single Green Method. This confirms the prediction at the end of section 3.2.1.

4.2 The Double Green Method

For the Double Green Method no results were obtained due to the finite time-span of the project, an overabundance of run-time errors in the FORTRAN code implementing the Double Green method and a lack of ability regarding the author to parse and resolve said run-time errors in a timely fashion.

Chapter 5

Discussion and Conclusion

5.1 Comparison of the Single and Double Green methods

As mentioned in section 3.2.1 the Single Green (SG) method cannot account for interactions between orbitals of electrons with different spin. And therefore any spin polarisation that arises by using this method must be an expression of the Zeeman effect. Thus one would only expect to see spin polarisation arise in these calculations when an external magnetic field would be applied, the contacts would be ferromagnetic. Spin-orbit interactions should also give rise to some spin-polarisation, but the way the SG-method is implemented into ADF at the moment does not work with a molecule that was prepared using a ZORA-DFT run configured to account for spin-orbit interactions.

Therefore the Double Green (DG) method was implemented to account for interactions between orbitals occupied by electrons of different spin and to be able to work alongside the ZORA Dirac Equation configured for spin-orbit interactions. By doing this some extra sources for the observed spin-polarisation can be identified. Because of some overlap between the spin-A and spin-B orbitals, spin-flip processes could occur. If these spin-flips do not occur symmetrically a non-zero spin polarisation would be measured.

One of the causes of these spin-flips could be the transmission of electrons from the gold contact to the Helicene via the sulfur atom. Gold has a heavy nucleus (Atom number $Z = 79$), and thus spin-orbit effects are relevant. When the atoms are transmitted to the molecule, the spin-A and spin-B would be transmitted at different energies which could cause some spin-polarisation.

Furthermore when the electrons travel through a Helical molecule they will follow a somewhat circular path when looking down the center line of the molecule. This would make a helical molecule act like a little solenoid when a current is applied, causing a magnetic effect which in turn could cause some spin-polarisation.

5.2 Implementation of the Double Green Method

ADF is a program written in FORTRAN, one of the first true scientific programming languages. In the thesis of Marnix Rebergen [11], the code was implemented in ADF2016 and was working and providing results that agree with experiment. But now the Double Green method is implemented in ADF2019. The relevant code was changed to implement the DG method. After compiling, however, some run-time errors would still shut down the calculation. Due to the finite nature of the project, not all errors were remedied before the end. Due to this no results were obtained for the DG method.

5.3 Conclusion of this research

As expected a Single Green method calculation can not simulate the CISS effect and therefore the Double Green method should be implemented in ADF. During the time of this research the author was not able to successfully do this and no results were obtained to confirm the ability of the Double Green method to be able to simulate the CISS effect. But since in the thesis of Marnix Rebergen [11] the same method was applied to a similar geometry resulting in spin polarisation agreeable to observations there is good confidence that the DG method implemented in ADF2019 will prove successfully as well.

Bibliography

[1] Evert Jan Baerends, Tom Ziegler, A. J. Atkins, Jochen Autschbach, Donald Bashford, O. Baseggio, A. Bérces, F. Matthias Bickelhaupt, C. Bo, P. M. Boerritger, Luigi Cavallo, C. Daul, D. P. Chong, D. V. Chulhai, L. Deng, R. M. Dickson, J. M. Dieterich, D. E. Ellis, M. van Faassen, A. Ghysels, A. Giammona, Stan J. A. van Gisbergen, A. Goez, A. W. Götz, S. Gusarov, F. E. Harris, P. van den Hoek, Z. Hu, Christoph R. Jacob, H. Jacobsen, L. Jensen, L. Joubert, J. W. Kaminski, G. van Kessel, C. König, F. Kootstra, A. Kovalenko, Mykhaylo Krykunov, Erik van Lenthe, D. A. McCormack, A. Michalak, M. Mitoraj, S. M. Morton, Johannes Neugebauer, V. P. Nicu, Louis Noodleman, V. P. Osinga, S. Patchkovskii, Michele Pavanello, C. A. Peeples, Pierre Herman Theodoor Philipsen, D. Post, Cory C. Pye, H. Ramanantoanina, P. Ramos, W. Ravenek, J. I. Rodríguez, P. Ros, R. Rüger, P. R. T. Schipper, D. Schlüns, H. van Schoot, G. Schreckenbach, J. S. Seldenthuis, Mike Seth, Jaap G. Snijders, Miquel Solà, Stener M., M. Swart, D. Swerhone, G. te Velde, V. Tognetti, P. Vernooijs, L. Versluis, Lucas Visscher, O. Visser, Fan Wang, T. A. Wesolowski, E. M. van Wezenbeek, G. Wiesenekker, S. K. Wolff, T. K. Woo, and A. L. Yakovlev. ADF2019, SCM, Theoretical Chemistry, Vrije Universiteit, Amsterdam, The Netherlands, https://www.scm.com, 2019.

[2] C. Fonseca Guerra, J. G. Snijders, G. te Velde, and E. J. Baerends. Towards an order-n dft method. *Theoretical Chemistry Accounts*, 99(6):391–403, Nov 1998.

[3] J. J. Thomson M.A. F.R.S. Xl. cathode rays. *The London, Edinburgh, and Dublin Philosophical Magazine and Journal of Science*, 44(269):293–316, 1897.

[4] B. Göhler, V. Hamelbeck, T. Z. Markus, M. Kettner, G. F. Hanne, Z. Vager, R. Naaman, and H. Zacharias. Spin selectivity in electron transmission through self-assembled monolayers of double-stranded dna. *Science*, 331(6019):894–897, 2011.

[5] D.J. Griffiths. *Introduction to Quantum Mechanics.* Prentice Hall, 2 edition, 2004.

[6] John Kerr LL.D. Xl. a new relation between electricity and light: Dielectrified media birefringent. *The London, Edinburgh, and Dublin Philosophical Magazine and Journal of Science*, 50(332):337–348, 1875.

[7] Ron Naaman and David H. Waldeck. Spintronics and chirality: Spin selectivity in electron transport through chiral molecules. *Annual Review of Physical Chemistry*, 66(1):263–281, 2015. PMID: 25622190.

[8] K. Padmaraju. Faraday rotation, 2008.

[9] W. Pauli. Über den zusammenhang des abschlusses der elektronengruppen im atom mit der komplexstruktur der spektren. *Zeitschrift für Physik*, 31(1):765–783, Feb 1925.

[10] M. Paulsson. Non equilibrium green's functions for dummies: Introduction to the one particle negf equations, 2008.

[11] M. Rebergen. A study of induced spin selectivity in chiral molecules. Master's thesis, Delft University of Technology, 2018.

[12] SCM. Green: Non-self-consistent green's function calculation. webpage. URL:`https://www.scm.com/doc/ADF/Input/GREEN.html`.

[13] J.S. Seldenthuijs. *Electrical and Mechanical Effects in Single-Molecule Junctions.* PhD thesis, Delft University of Technology, 2011.

[14] G. te Velde, F. M. Bickelhaupt, E. J. Baerends, C. Fonseca Guerra, S. J. A. van Gisbergen, J. G. Snijders, and T. Ziegler. Chemistry with adf. *J. Comput. Chem.*, 22(9):931–967, 2001.

[15] A. Teepe. Bachelor end project: A study of chiral induced spin selectivity by means of a computer simulation, 2019.

[16] J. Thijssen. *Computational Physics.* Cambridge University Press, 2 edition, 2007.

[17] A.J Kox & W.P. Troelstra. Uit het zeeman-archief: De ontdekking van het zeeman effect. *Gewina 19*, pages 153–166, 1996.

[18] S. Goudsmit & G. Uhlenbeck. Spinning electrons and the structure of spectra. *Nature*, 117(2938):264–265, Feb 1926.

[19] Zouti Xie, Tal Z. Markus, Sidney R. Cohen, Zeev Vager, Rafael Gutierrez, and Ron Naaman. Spin specific electron conduction through dna oligomers. *Nano Letters*, 11(11):4652–4655, 2011. PMID: 21961931.

[20] P. Zeeman. The effect of magnetisation on the nature of light emitted by a substance. *Nature*, 55(1424):347, 1897.